R13, a TrkB Agonist Prodrug, Inhibits Asparagine Endopeptidase (AEP) and Increases Osteoprotegerin (OPG), Preventing Bone Loss

Jing Xiong
Emory University
Xia Liu
Emory Universtity
Zhaohui Zhang
Wuhan University
Jonathan Adams
Emory university
Roberto Pacifici
Emory University https://orcid.org/0000-0001-6077-8250
Keqiang Ye (kye@emory.edu)
Emory University https://orcid.org/0000-0002-7657-8154

Article

Keywords: BDNF, TrkB, R13, osteoporosis

Posted Date: April 23rd, 2021

DOI: https://doi.org/10.21203/rs.3.rs-412961/v1

Version of Record: A version of this preprint was published at Nature Communications on August 16th, 2022. See the published version at https://doi.org/10.1038/s41467-022-32435-5.

R13, a TrkB Agonist Prodrug, Inhibits Asparagine Endopeptidase (AEP) and Increases Osteoprotegerin (OPG), Preventing Bone Loss

By

Jing Xiong[1,2], Xia Liu[1], Zhaohui Zhang[2], Jonathan W. Adam[3], Roberto Pacifici[3] and Keqiang Ye[1, #]

[1]Department of Pathology and Laboratory Medicine,

[3]Division of Endocrinology, Metabolism and Lipids, Department of Medicine,

Emory University School of Medicine

Atlanta, GA 30322,

USA

[2]Department of Neurology, Renmin Hospital of Wuhan University,

Wuhan 430060, Hubei Province, P. R. China

[#]To whom all correspondence should be addressed (E-mail: kye@emory.edu)

Keywords: neurotrophins; C/EBPβ; AEP; RANKL; OPG; Bone loss

Abstract

Brain-derived neurotrophic factor (BDNF) and its tropomyosin-related kinase B receptor (TrkB) are expressed in human osteoblasts and mediate fracture healing. BDNF/TrkB signaling activates Akt that phosphorylates and inhibits asparagine endopeptidase (AEP), which regulates the differentiation fate of human bone marrow stromal cells (hBMSC) and is altered in postmenopausal osteoporosis. Here we show that R13, a small molecular TrkB receptor agonist prodrug, inhibits AEP and promotes bone formation. Though both Receptor activator of nuclear factor kappa-B ligand (RANKL) and Osteoprotegerin (OPG) induced by ovariectomy (OVX) remain comparable between WT and BDNF +/- mice, R13 treatment significantly elevates OPG in both mice without altering RANKL, blocking trabecular bone loss. Moreover, OVX increases RANKL and OPG in WT and AEP KO mice with RANKL/OPG ratio lower in the latter than the former, attenuating bone turnover. 7,8-DHF, released from the prodrug R13, activates TrkB and its downstream effector CREB, which is critical for OPG augmentation. Consequently, 7,8-DHF represses C/EBPβ/AEP pathway, inhibiting RANKL-induced RAW264.7 osteoclastogenesis. Therefore, our findings support that R13 exerts its therapeutic efficacy toward osteoporosis via inhibiting AEP and escalating OPG.

Introduction

Brain-derived neurotrophic factor (BDNF) belongs to the family of neurotrophins that play essential roles in the central nervous system (CNS) and are mainly expressed in central and

peripheral neuronal tissues [1,2]. However, BNDF is also synthesized and released from non-neuronal cells such as fibroblasts, osteoblasts, endothelial cells, monocytes and mast cells [3,4]. Plasma BDNF levels are increased in patients with osteoarthritis compared to healthy individuals [5]. BDNF is involved in osteoblast cell differentiation and stimulates bone/cementum-related proteins including alkaline phosphatase (ALP), bone morphogenetic protein-2 (BMP-2) and osteopontin (OPN) expression in cementoblasts[6]. Both BDNF and its TrkB receptor are present at various stages of the bone formation process, and they are upregulated in human osteoblasts and implicated in fracture healing [7]. BDNF strongly elevates mRNA expression of the osteoblast differentiation marker, osteocalcin, in the osteoblast-lineage cell MC3T3-E1 and stimulates cell differentiation and promotes new bone formation and maturation [8].

AEP (asparaginyl endopeptidase, also known as legumain with gene name: *LGMN*) is a broadly expressed endo-lysosomal cysteine protease that is secreted as inactive pro-zymogen (56 kDa) and processed into an enzymatically active 36 kDa mature form and a 17 kDa C-terminal inhibitory fragment [9]. Strikingly, the C-terminal truncate inhibits osteoclast differentiation through binding to an uncharacterized receptor [10,11]. Active AEP inhibits osteoblast differentiation and *in vivo* bone formation through degradation of the bone matrix protein, fibronectin. During development, AEP-deficient zebrafish exhibits precocious bone formation and mineralization [12]. Human bone marrow stromal cells (hBMSCs) are non-hematopoietic multipotent cells capable of differentiation into mesodermal cell types such as osteoblasts and adipocytes [13]. Markedly, AEP regulates the lineage commitment of hBMSCs

and is abnormally expressed and displays aberrant subcellular localization in the bone from patients with postmenopausal osteoporosis[12].

We have described 7,8-dihydroxyflavone (7,8-DHF) as a small molecule that mimics BDNF and acts as a specific TrkB agonist with high binding affinity. After binding to the extracellular motif on TrkB receptor, 7,8-DHF triggers receptor dimerization and auto-phosphorylation, initiating neurotrophic activities [14-16]. It is well documented that 7,8-DHF simulates BDNF biologic functions and exerts promising therapeutic efficacy toward a variety of diseases implicated with BDNF/TrkB signaling [17-20]. To improve its *in vivo* pharmacokinetic (PK) profiles, we have prepared a prodrug, R13, that releases 7,8-DHF after absorption and significantly increases its oral bioavailability[21-23]. Recently, we reported that BDNF/TrkB signaling inhibits AEP via Akt phosphorylation of the T322 residue, suppressing AEP activation[24]. Oral administration of R13 elicits robust TrkB receptor activation in the brain and the gut and inhibits AEP via Akt-mediated T322 phosphorylation [21]. Moreover, C/EBPβ is a pivotal transcription factor for escalating AEP expression during age [25], and activation of the BDNF/TrkB pathway represses C/EBPβ/AEP signaling [26].

Osteoporosis is a systemic bone disease, characterized by reduced bone mass, and disruption of normal bone architecture, resulting in bone fragility and increased risk of fractures [27]. Bone homeostasis depends on the resorption of bones by osteoclasts and formation of bones by the osteoblasts. Osteoblasts can also affect osteoclast formation, differentiation, or apoptosis through several pathways, such as OPG/RANKL/RANK. In the current study, to

test the hypothesis that the BDNF mimetic drug R13 may block AEP and promote bone formation, we employed BDNF +/-, AEP -/- and wild-type (WT) littermate mice and examined their roles in ovariectomy (OVX)-induced bone loss in the presence or absence of R13. We found that AEP KO decreased OVX-induced bone loss via increasing osteoblast formation and inhibiting osteoclast formation. 7,8-DHF, the active pharmaceutical ingredient released from R13, elevates OPG expression via activating CREB and blocks RANKL-induced osteoclastogenesis. R13 not only represses AEP expression through blunting its upstream transcription factor C/EBPβ but also blocks AEP activation via BDNF/TrkB pathway-activated Akt and it displays promising therapeutic efficacy toward osteoporosis.

Results

Knockout of AEP improves trabecular bone density in ovariectomized female mice

To explore the role of AEP in bone remodeling, we subjected AEP knockout mice (AEP KO) and WT littermates to OVX at the age of 12 weeks. As expected, the shrunken uterine morphology and reduced uterus weight revealed that OVX surgery was successful (Supplementary Figure 1). Microcomputed tomography (μCT) analysis of femurs harvested at sacrifice revealed a higher trabecular bone volume fraction (BV/TV), Conn.D and a lower Structure model index (SMI) in AEP KO mice compared with AEP WT mice after OVX. Moreover, OVX decreased trabecular number (Tb.N) and increased trabecular separation (Tb.Sp), while trabecular thickness (Tb.Th) indices were similar among the groups. These indices remained similar between two types of mice under sham operation (Figure 1A & B). Notably, levels of serum osteocalcin, a marker of bone formation, were increased after OVX

with AEP KO significantly higher than WT. The serum [BDNF]s were comparable among the 4 groups. Quantification of bone resorption indices in the serum showed that the concentrations of C-terminal telopeptide of collagen (CTX), a marker for bone resorption, and RANKL were increased after OVX mice. Moreover, OPG concentrations were much higher in AEP KO mice than WT mice under both OVX and sham conditions, suggesting that AEP antagonizes OPG expression under the physiological condition. Consequently, the ratios of RANKL/OPG were substantially higher in OVX groups than sham groups with AEP KO mice lower than WT mice, in alignment with higher bone density in AEP KO group versus WT group after OVX (Figure 1C). Hence, AEP deletion diminishes the ratio of RANKL/OPG, leading to increased trabecular bone density after OVX.

Deletion of AEP inhibits the bone turnover induced by ovariectomy

To further characterize the roles of AEP in OVX-induced osteoporosis, we performed the H&E staining and analyzed the bone morphology and white adipocytes in both animals after OVX surgery. White adipocytes were evidently reduced in the bone from AEP KO mice after OVX as compared to WT mice (Figure 2A). Tartrate-resistant acid phosphatase (TRAP) staining revealed that OVX induced more osteoclast cells in WT than AEP KO mice (Figure 2B). Based on dynamic indices of femur trabecular bone formation, no significant difference in mineral apposition rate (MAR) and bone formation rate (BFR) was found between WT and AEP KO sham mice, but OVX decreased the BFR in WT mice as compared with AEP KO mice (Fig. 2D). Analysis of static indices of bone formation and resorption revealed that both number of osteoclasts (N. Oc/BS) and the percentage of surfaces covered by osteoclasts

(OcS/BS) were greatly decreased in AEP KO mice compared with WT mice after OVX. On the other hand, OVX also elicited a compensatory increase of number of osteoblasts (N. Ob/BS) in AEP WT group but not in AEP KO mice (Figure 2D). Together, these data suggest that AEP deficient mice exhibit a higher bone formation and a lower bone resorption after OVX.

R13 increases OPG levels and blocks trabecular bone loss induced by ovariectomy

To explore the biological roles of BDNF/TrkB signaling in OVX-induced bone loss, we employed 3 months old female BDNF +/- mice and WT littermates. One week after OVX surgery, WT and BDNF +/- mice were administered either R13 (21.8 mg/kg) or vehicle, orally, six days per week for eight weeks. Assessment of femoral bone structure by *in vitro* μCT revealed that trabecular bone volume, expressed as a function of total tissue volume fraction (BV/TV) was dramatically decreased by OVX in both WT and BDNF +/- mice. R13 treatment increased BV/TV. Quantification of parameters of trabecular structure revealed that R13-treated mice displayed higher trabecular thickness (Tb.Th) than vehicle control and trabecular number (Tb.N), decreased trabecular spacing (Tb.Sp) in both type of mice as compared with the OVX-treated group (Figure 3A & B). Assessments of the serum levels of CTX and osteocalcin indicated osteocalcein was increased in R13-treated OVX mice compared with vehicle-treated OVX group, and both strains of OVX-treated mice exhibited higher CTX level compared to the sham group. Nevertheless, OPG were substantially increased upon R13 treatment, leading to significant reduction RANKL/OPG ratios in both WT and BDNF +/- mice, though the serum BDNF levels remained equivalent among the

groups (Figure 3C). Hence, BDNF haploinsufficiency does not alter femur trabecular bone properties after OVX, but treatments with R13 strongly increase bone density.

R13 blocks the changes in bone turnover induced by ovariectomy

To further explore the roles of BDNF signaling in bone resorption and formation after OVX, we conducted H&E staining and analyzed bone morphology and white adipocytes in both WT and BDNF+/- mice after OVX surgery. Cleary, R13 treatment decreased the adipocyte content in the bone after OVX (Figure 4A). TRAP staining revealed that OVX-induced demonstrable osteoclast cells in both WT and BDNF +/- mice were diminished by R13 treatments (Figure 4B). Calcein double-fluorescence labeling allows the determination of the onset time and location of mineralization and the direction and speed of bone formation. Interestingly, R13 vigorously increased these parameters in both WT and BDNF +/- mice (Figure 4C), indicating that OVX-induced bone loss is attenuated by R13 treatment via an increase in bone formation. Dynamic indices of bone formation showed that vehicle-treated mice exhibited lower MAR and BFR as compared to R13-treated mice. By contrast, no significant differences in ObS/BS and N.Ob/BS, which are static indices of bone formation, were found in vehicle and R13-treated mice. Treatments with R13 inhibited N.Oc/BS in both WT and BDNF +/- mice after OVX. Nonetheless, the percentage of surfaces covered by OCs (Oc.S/BS) remained comparable among the groups regardless of the treatment (Figure 4D). Hence, these data support that R13 treatment induces bone formation and inhibits bone resorption after OVX. Remarkably, R13 significantly increased OPG levels without affecting RANKL and it also elevated BV/TV ratio in WT mice without any surgery (Supplementary

Figure 2). Thus, R13 treatment greatly blocks the bone loss induced by OVX and substantially elevates OPG levels.

7,8-DHF promotes MC3T3-E4 cell differentiation, mineralization and OPG secretion

7,8-DHF binds to TrkB receptor extracellular region, where BDNF interacts on the TrkB receptors [28], mimicking the biological actions of BDNF in a TrkB-dependent manner[29,30]. To examine the molecular mechanisms of how 7,8-DHF stimulates bone density elevation in rodents, we tested its effect in MC3T3-E1 cells in the presence of OIM (osteogenic induction medium). Alkaline phosphatase (ALP) staining showed that OIM treatment at 14 days evidently enhanced osteoblast cell differentiation, which was further escalated by BDNF or 7,8-DHF, respectively. Alizarin Red staining also validated these observations at 21 days (Figure 5A & B), supporting the conclusion that BDNF or 7,8-DHF strongly stimulates MC3T3-E1 differentiation and calcium deposition.

Stimulation of the BDNF/TrkB pathway inhibits AEP activation via Akt phosphorylation of T322 residue, sequestering AEP into the lysosomes[24] and decreases AEP expression levels via repressing its transcription factor C/EBPβ[26]. Immunoblotting revealed that OIM robustly induced p-C/EBPβ and total C/EBPβ expression in MC3T3-E1 cells, both of which were distinctly repressed by either BDNF or 7,8-DHF. Consequently, expression of the downstream effector, AEP, was clearly diminished, which inversely associated with RANKL and OPG augmentation. Osterix, a key early gene in the bone formation cascade, is usually used as a predictive measure of bone formation. As expected, OIM prominently elevated

Osterix levels as compared with vehicle. The similar findings occurred in the presence of BDNF or 7,8-DHF (Figure 5C & D). In alignment with active AEP repression by BDNF or 7,8-DHF, the enzymatic assay validated that AEP protease activities were greatly blocked (Figure 5E).

To further interrogate the role of AEP in MC3T3-E1 cell differentiation and mineralization induced by OIM, we transfected the cells with dominant-negative enzymatic-dead AEP C189S mutant, and found that blockade of AEP highly escalated fibronectin, Osterix and RUNX2 (Supplementary Figure 3A & D). ALP staining and Alizarin Red S analysis showed that antagonizing AEP strongly promoted osteoblast cell differentiation and bone formation (Supplementary Figure 3B & C). As expected, AEP C189S mutant robustly inhibited OIM-elicited AEP activities (Supplementary Figure 3E). Quantitative RT-PCR (qRT-PCR) analysis revealed that 7,8-DHF exhibited the strongest stimulatory effect in promoting OPG mRNA levels, followed by BDNF and OIM. On the other hand, BDNF triggered the most RANKL mRNA transcription (Figure 5F). Both OPG and RANKL protein levels were elevated by OIM in ELISA assays. These elevations were further augmented in the presence of 7,8-DHF or BDNF (Figure 5G, left two panels), consistent with the findings in Western blotting. Though both RANKL and OPG concentrations were substantially elevated by BDNF and 7,8-DHF, the ratio of RANKL/OPG triggered by OIM alone was significantly higher than 7,8-DHF (Figure 5F, right panel). Together, these observations strongly support that 7,8-DHF mimics BDNF and that both strongly escalate OPG expression and decrease RANKL/OPG ratio, accelerating osteoblast formation. Moreover, it also represses the

C/EBPβ/AEP pathway, leading to inhibition of osteoclast formation.

7,8-DHF increases OPG expression via activating transcription factor CREB

To further interrogate the molecular mechanism of 7,8-DHF in promoting OPG expression, we conducted a time course study in MC3T3-E1 cells in the presence of OIM. As expected, 7,8-DHF swiftly activated p-TrkB and its downstream effectors p-MAPK and p-Akt, supporting that 7,8-DHF indeed mimics BDNF by activating TrkB neurotrophic signaling. Numerous transcription factors including c-Jun and CREB have been shown to be implicated in OPG mRNA transcription [31,32]. Noticeably, p-C/EBPβ, p-c-Jun and p-CREB signals were time-dependently increased by 7,8-DHF (Figure 6A & B), suggestive of the activation of these transcription factors. To examine which of them are essential for OPG expression, we knocked down each of them in MC3T3-E1 cells via the specific siRNAs in the presence of OIM and 7,8-DHF. Consistently, OIM manifestly increased OPG and RANKL, associated with C/EBP and c-Jun augmentation, whereas CREB total level remained constant. Again, 7,8-DHF treatment attenuated C/EBPβ without interfering CREB or c-Jun levels. Remarkably, knocking down CREB or c-Jun but not C/EBPβ clearly reduced OPG protein levels, and the ratio of RANKL/OPG was significantly augmented when CREB was depleted (Figure 6C & D). qRT-PCR demonstrated that 7,8-DHF-stimulated OPG mRNA was selectively suppressed when CREB was knocked down by its siRNA, whereas RNAKL mRNA levels were similar among the groups, resulting in higher RANKL/OPG ratio (Figure 6E). Hence, 7,8-DHF via activating CREB, a well-characterized downstream transcription factor of BDNF/TrkB pathway, stimulates OPG expression levels.

240

241 **7,8-DHF inhibits RANK-L-induced RAW264.7 osteoclastogenesis**

242 RAW264.7 cell is a well-established cellular model for osteoclastic differentiation, which has
243 been widely engaged in bone homeostasis research. Moreover, RANKL independently
244 induces RAW264.7 cell osteoclastic differentiation, which efficiently generates osteoclasts *in*
245 *vitro* [33]. To investigate whether the promotion of bone formation by 7,8-DHF also might
246 involve inhibiting osteoclastogenesis, we employed RAW264.7 cells in the presence of
247 RANKL. Treatment with 30 ng/ml RANKL at day 4 significantly increased the number of
248 multinucleated osteoclastic cells and this increase was diminished by addition of BDNF or
249 7,8-DHF, indicating the inhibition of the ability of RANKL to promote osteoclastogenesis
250 (Supplementary Figure 4A). Immunoblotting analysis revealed that C/EBPβ was greatly
251 reduced by 7,8-DHF or BDNF treatments, and RANKL-stimulated AEP oscillated the
252 upstream C/EBPβ levels (Supplementary Figure 4B & C). Hence, 7,8-DHF blocks RANKL-
253 induced RAW264.7 osteoclastogenesis associated with AEP inhibition.

254

255

256 **Discussion**

257 BDNF stimulates mRNA expression of the osteoblast differentiation marker, osteocalcin, and
258 promotes the differentiation of MC3T3-E1 cells, augmenting new bone formation and
259 maturation [8]. Both BDNF and its TrkB receptor are demonstrable in various stages of the
260 bone formation process in human fracture gap tissues and upregulated in human osteoblasts
261 [7]. However, we found that BDNF +/- mice fail to exhibit any significant difference in bone

loss from WT littermates upon OVX, indicating that endogenous BDNF/TrkB pathway might be dispensable in preventing bone loss triggered by OVX. Nevertheless, TrkB receptor agonist R13 treatment substantially elevates OPG and reduces RANKL/OPG ratios in both WT and BDNF +/- mice after OVX, leading to prominent bone density augmentation (Figure 5&6). Previous study shows that central BDNF deletion produces a marked skeletal phenotype characterized by increased femur length, elevated whole bone mineral density, and bone mineral content. Moreover, the skeletal changes are developmentally regulated and appear concurrently with the metabolic phenotype, suggesting that the metabolic and skeletal actions of BDNF are linked[34]. Nonetheless, we did not find any significant bone alteration in BDNF +/- mice as compared to WT littermates (Figure 3). Presumably, complete BDNF knockout in the CNS may disrupt the endocrine hormones that mediate the metabolism and bone homeostasis.

The proinflammatory cytokines (e.g., TNF-α and IL-6) are upregulated in osteoporotic bone marrow microenvironment [35]. These cytokines activate the transcription factor C/EBPβ, which feeds back and acts as transcription factor for these cytokines as well [36]. Most recently, we show that BDNF and C/EBPβ mutually regulate each other negatively. For instance, BDNF deficiency increases production of inflammatory cytokines and activates the JAK2/STAT3 pathway, resulting in the upregulation of transcription factor C/EBPβ [26]. In turn, C/EBPβ acts a repressor that binds to BDNF exon IV promoter and blocks BDNF mRNA transcription[37]. Treatments with BDNF and 7,8-DHF thus pronouncedly diminish C/EBPβ expression, leading to AEP reduction, which is inversely correlated with RANKL

and OPG escalation (Figure 5&6; supplementary Figure 4). Interestingly, we observed OPG elevation in AEP KO mice as compared to WT mice under sham condition (Fig 1C), suggesting that AEP somehow physiologically represses OPG expression. Previously, we reported that AEP cuts α-Synuclein N103 and Tau N368, which bind to the TrkB receptor intracellular domain and inhibit the neurotrophic activities[38,39]. Conceivably, AEP antagonizes BDNF/TrkB neurotrophic signalings, leading to OPG suppression. Depletion of AEP consequently alleviates the inhibition and escalates OPG expression. OPG plays a suppressive role in cytokine-induced osteoclastogenesis [40]. Moreover, both CREB and c-fos transcription factors mediate OPG and RANKL mRNA expression[31]. Notably, CREB, a crucial downstream transcription factor of BDNF/TrkB pathway, plays a pivotal role in mediating 7,8-DHF-stimulated OPG escalation, though all of transcription factors including C/EBPβ, c-Jun and CREB are phosphorylated upon 7,8-DHF treatment, accompanied by p-TrkB and its downstream effectors escalation (Figure 6A & B). Thus, 7,8-DHF-triggered p-CREB is indispensable for augmenting OPG expression and osteoblast differentiation.

AEP is a secreted cysteine protease involved in diverse biological processes. The proteolytic activity of AEP is important for its effects on hBMSC differentiation and bone formation, and AEP inhibits osteoblast cell differentiation through degradation of fibronectin[12]. AEP expression is elevated in hBMSCs from osteoporotic patients and, at single-cell resolution, and AEP overexpression in adipocyte differentiation is inversely correlated with local trabecular bone volume. Recently, we have reported that C/EBPβ upregulates AEP expression during aging [25]. BDNF or 7,8-DHF robustly represses C/EBPβ expression induced by OIM

(Osteogenic induction medium) or RANKL, resulting in AEP reduction and its protease activity repression. Consequently, 7,8-DHF strongly blocked RANK-L induced RAW264.7 osteoclastogenesis (Supplementary Figure 4). Remarkably, we have recently reported that 7,8-DHF decreases follicle stimulatory hormone (FSH) production, resulting in increased serum estradiol in female mice treated with HFD [41]. Previously, it has been reported that FSH triggers bone loss and anti-FSH increased bone density without altering estrogen concentrations[42,43]. It is possible that FSH might somehow activate AEP and trigger bone loss. Imaginably, 7,8-DHF represses FSH production, resulting in AEP inhibition and bone density increase. Clearly, the data presented above, combined with AEP KO mice display diminished bone loss upon OVX and reduced RANKL/OPG ratios, strongly support the conclusion that R13 may ameliorate OVX-induced bone loss via antagonizing AEP and elevating OPG (Figure 6F).

Methods

Animals

Female C57BL6/J wild-type mice and BDNF+/- mice were obtained from Jackson Laboratory (MMRRC stock#000664 and 002267), then held and underwent breeding at Emory School of Medicine. The AEP knockout mice on a mixed C57BL/6 and 129/Ola background were generated as reported [44]. All *in vivo* experiments were carried out in female mice. All mice were kept under specific pathogen free conditions in an environmentally controlled clean room and housed at 22 °C on a 12-h/12-h light/dark cycle. Food and water were provided *ad lib*. The experiments were conducted according to the NIH animal care

guidelines and Emory School of Medicine guidelines. The protocol was reviewed and approved by the Institutional Animal Care and Use Committee (IACUC) at Emory University. WT, BDNF+/- mice, AEP WT and AEP knockout mice were bilaterally ovariectomized or sham operated at 12 weeks of age. One weeks after ovariectomy, the WT and BDNF+/- mice received vehicle or R13 dissolved in 5% DMSO/0.5% methylcellulose at dose of 21.8mg/kg/d, six days per week, for 8 weeks by gavage.

Cell culture. Murine MC3T3-E1 (subclone 4) cells and RAW 264.7 cells were obtained from American Type Culture Collection (ATCC, Manassas, VA, USA). The MC3T3-E1 cells were cultured in alpha-MEM (Gibco, cat. A1049001) with 10% FBS and 0.1% penicillin /streptomycin, but without ascorbic acid. The RAW 264.7 cells were cultured in DMEM supplemented with 10% FBS and 0.1% penicillin-streptomycin. The cells were maintained at 37°C in a humidified atmosphere of 95% air and 5% CO2.

Osteogenic differentiation. MC3T3-E1 cells were seeded into plates in complete medium and cultured for 24 days until the cells reached 70% confluence. To initiate the differentiation, the cells were incubated in osteogenic induction medium (OIM) containing α-MEM, 10% FBS, dexamethasone (10-7M), β-glycerophosphate (10 mM) and ascorbic acid (50 μg/ml). The differentiation medium was replaced every 3 days, with DMSO, BDNF (50 ng/ml) or 7,8 DHF (0.5 μM) added into the medium. The MC3T3-E1 cells were transfected with AEPC189S plasmid, C/EBP β siRNA (sc-29862, Santa Cruz Biotechnology, USA), CREB siRNA (sc-35111, Santa Cruz Biotechnology, USA), C-Jun siRNA (sc-29224, Santa

Cruz Biotechnology, USA) or control plasmid or control-siRNA (sc-44237, Santa Cruz Biotechnology, USA) by Lipo3000 transfection reagent (Invitrogen, USA) according to the instructions.

Osteoclast differentiation. RAW264.7 cells were seeded in 24 wells plates and cultured for 24 hours in DMEM with 10% FBS and 0.1 penicillin/streptomycin. The medium was changed to α-MEM with 5% FBS, 0.1% penicillin/streptomycin. The receptor activator of NF-κB ligand (RANKL, 30 ng/ml) was added to induce osteoclast differentiation. The medium was replaced every 3 days, accompanied with DMSO, BDNF (50 ng/ml) or 7,8 DHF (0.5 μM) added into the medium.

ALP staining. MC3T3-E1 cells were plated in 24-well plates, cultured in complete medium or OIM, and treated with BNDF (50 ng/ml) or 7,8 DHF (0.5 μM) for 14 days. The Cells were washed in PBS twice, and fixed for 10 minutes with fixing buffer at room temperature, stained the ALP staining with the TRACP&ALP double-staining kit (TaKaRa, Japan, Cat. #MK300)

Alizarin Red S staining. MC3T3-E1 cells were treated with OIM, OIM + BDNF (50 ng/ml) or OIM + 7,8 DHF (0.5 μM), and left untreated for 21 days, and then were washed in distilled water twice and fixed in 70% ice-cold ethanol. Then the cells were stained with 2% Alizarin Red S solution (Sigma, St. Louiss, MO, USA) to detect calcification.

TRAP staining. RAW 264.7 cells were cultured in α-MEM with or without RANKL, in the presence or absence of BNDF (50 ng/ml) or 7,8 DHF (0.5 μM) for 5 days. The cells were washed in PBS twice, fixed in fixing solution for 10 minutes at room temperature, and then stained the TRAP activity with the TRACP&ALP double-staining kit (TaKaRa, Japan, Cat. #MK300) according to the supplied protocols.

Western blotting. MC3T3-E1 and RAW 264.7 cells were washed with ice-cold PBS and lysed in (50 mM Tris, pH 7.4, 40 mM NaCl, 1 mM EDTA, 0.5% Triton X-100, 1.5 mM Na3VO4, 50 mM NaF, 10 mM sodium pyrophosphate, 10 mM sodium β-glycerophosphate, supplemented with protease inhibitors cocktail) at 4°C for 0.5 h, and centrifuged for 25 min at 15,000 rpm. The supernatant was boiled in SDS loading buffer. After SDS-PAGE, the samples were transferred to a nitrocellulose membrane. The membrane was blocked with TBS containing 5% nonfat milk and 0.1% Tween 20 (TBST) at room temperature for 2 hours, followed by the incubation with primary antibody at 4°C overnight, and with the secondary antibody at room temperature for 2 hours. After washing with TBST, the membrane was developed using the enhanced chemiluminescent (ECL) detection system.

AEP activity assay. Cell lysates (10 μg) were incubated in 200 μl assay buffer (20 mM citric acid, 60 mM Na2HPO4, 1 mM EDTA, 0.1% CHAPS, and 1 mM DTT, pH 6.0) containing 20 μM δ-secretase substrate Z-Ala-Ala-Asn-AMC (Bachem). AMC released by substrate cleavage was quantified by measuring at 460 nm in a fluorescence plate reader at 37 °C for 2 h in kinetic mode.

Quantitative real-time PCR analysis. Total RNA was isolated by TRIzol (Life Technologies). Reverse transcription was performed with SuperScript III reverse transcriptase (Life Technologies). Gene-specific primers and probes were designed and bought from Taqman (Life Technologies). All real-time PCR reactions were performed using the ABI 7500-Fast Real-Time PCR System and the Taqman Universal Master Mix Kit (Life Technologies). The relative quantification of gene expression was calculated using the ΔΔCt method. We use predesigned real-time PCR primers from Applied Biosystems for the analysis of Opg (Tnfrsf11b; Mm0043545_m1), Rankl (Tnfsf11; Mm00441908_m1), AEP (Lgmn; Mm01325350_m1), GAPDH (Gapdh; Mm99999915_g1).

μCT measurements. μCT scan and analysis was performed in femurs *ex vivo* using a μCT-40 scanner, as previously reported[45,46]. Voxel sizes were 12 μm^3 for the *in vitro* measurements of femurs. For the femoral trabecular region, we analyzed 140 slices, beginning 50 slices below the distal growth plate. X-ray tube potential was 70 kVp, and integration time was 200 ms. Representative samples were reconstructed in 3D to generate visual representations of trabecular structure.

Quantitative bone histomorphometry. The measurements, indices and units for histomorphometric analysis were recommended by the Nomenclature Committee of the American Society of Bone and Mineral Research[47]. Mice were injected with calcein (25 μg/g) subcutaneously at day 10 and day 3 before sacrifice. Bone histomorphometric analysis

was performed at the University of Alabama at Birmingham Center for Metabolic Bone Disease-Histomorphometry and Molecular Analysis Core Laboratory. The Goldner's trichrome-stained plastic-embedded sections of calcein-double labeled femora of the mice were analyzed by an operator blinded as to the nature of the samples.

Biochemical markers of bone turnover. Serum Osteocalcin (Novus biologicals, Cat. NBP2-68151), CTX (Immunodiagnostic systems, Cat. AC-06F1), RANKL and OPG (Abcam, Cat. ab269553 and ab203365) were measured by specific Elisa assays.

ACKNOWLEDGEMENTS

This work was supported by grants from NIH grant (RF1, AG051538) to K. Y. The authors are thankful for Dr. Arthur W. English at Cell Biology Department at Emory University for critical proofreading the manuscript.

AUTHOR CONTRIBUTIONS

K.Y. conceived the project, designed the experiments, analyzed the data and wrote the manuscript. X.J. designed and performed most of the experiments. X.L. prepared the animal breeding. J.A. performed the in vitro bone CT analysis. Z.Z. and R.P. contributed to write the manuscript.

COMPETING FINANCIAL INTERESTS

The authors declare no competing financial interests.

References:

1 Huang, E. J. & Reichardt, L. F. Neurotrophins: roles in neuronal development and function. *Annu Rev Neurosci* **24**, 677-736, doi:10.1146/annurev.neuro.24.1.677 (2001).

2 Kaplan, D. R. & Miller, F. D. Neurotrophin signal transduction in the nervous system. *Curr Opin Neurobiol* **10**, 381-391, doi:10.1016/s0959-4388(00)00092-1 (2000).

3 Cartwright, M., Mikheev, A. M. & Heinrich, G. Expression of neurotrophin genes in human fibroblasts: differential regulation of the brain-derived neurotrophic factor gene. *Int J Dev Neurosci* **12**, 685-693, doi:10.1016/0736-5748(94)90048-5 (1994).

4 Labouyrie, E. *et al.* Expression of neurotrophins and their receptors in human bone marrow. *Am J Pathol* **154**, 405-415, doi:10.1016/S0002-9440(10)65287-X (1999).

5 Simao, A. P. *et al.* Involvement of BDNF in knee osteoarthritis: the relationship with inflammation and clinical parameters. *Rheumatol Int* **34**, 1153-1157, doi:10.1007/s00296-013-2943-5 (2014).

6 Kajiya, M. *et al.* Brain-derived neurotrophic factor stimulates bone/cementum-related protein gene expression in cementoblasts. *J Biol Chem* **283**, 16259-16267, doi:10.1074/jbc.M800668200 (2008).

7 Kilian, O. *et al.* BDNF and its TrkB receptor in human fracture healing. *Ann Anat* **196**, 286-295, doi:10.1016/j.aanat.2014.06.001 (2014).

8 Ida-Yonemochi, H., Yamada, Y., Yoshikawa, H. & Seo, K. Locally Produced BDNF Promotes Sclerotic Change in Alveolar Bone after Nerve Injury. *PLoS One* **12**, e0169201, doi:10.1371/journal.pone.0169201 (2017).

9 Dall, E. & Brandstetter, H. Structure and function of legumain in health and disease. *Biochimie* **122**, 126-150, doi:10.1016/j.biochi.2015.09.022 (2016).

10 Choi, S. J. *et al.* Identification of human asparaginyl endopeptidase (legumain) as an inhibitor of osteoclast formation and bone resorption. *J Biol Chem* **274**, 27747-27753, doi:10.1074/jbc.274.39.27747 (1999).

11 Choi, S. J., Kurihara, N., Oba, Y. & Roodman, G. D. Osteoclast inhibitory peptide 2 inhibits osteoclast formation via its C-terminal fragment. *J Bone Miner Res* **16**, 1804-1811, doi:10.1359/jbmr.2001.16.10.1804 (2001).

12 Jafari, A. *et al.* Legumain Regulates Differentiation Fate of Human Bone Marrow Stromal Cells and Is Altered in Postmenopausal Osteoporosis. *Stem Cell Reports* **8**, 373-386, doi:10.1016/j.stemcr.2017.01.003 (2017).

13 Abdallah, B. M. & Kassem, M. Human mesenchymal stem cells: from basic biology to clinical applications. *Gene Ther* **15**, 109-116, doi:10.1038/sj.gt.3303067 (2008).

14 Jang, S. W. *et al.* N-acetylserotonin activates TrkB receptor in a circadian rhythm. *Proc Natl Acad Sci U S A* **107**, 3876-3881, doi:10.1073/pnas.0912531107 (2010).

15 Liu, X. *et al.* A synthetic 7,8-dihydroxyflavone derivative promotes neurogenesis and exhibits potent antidepressant effect. *J Med Chem* **53**, 8274-8286, doi:10.1021/jm101206p (2010).

16 Liu, C., Chan, C. B. & Ye, K. 7,8-dihydroxyflavone, a small molecular TrkB agonist, is useful for treating various BDNF-implicated human disorders. *Transl Neurodegener* **5**, 2, doi:10.1186/s40035-015-0048-7 (2016).

17 Zhang, Z. *et al.* 7,8-dihydroxyflavone prevents synaptic loss and memory deficits in a mouse

model of Alzheimer's disease. *Neuropsychopharmacology* **39**, 638-650, doi:10.1038/npp.2013.243 (2014).

18 Devi, L. & Ohno, M. 7,8-dihydroxyflavone, a small-molecule TrkB agonist, reverses memory deficits and BACE1 elevation in a mouse model of Alzheimer's disease. *Neuropsychopharmacology* **37**, 434-444, doi:10.1038/npp.2011.191 (2012).

19 Castello, N. A. *et al.* 7,8-Dihydroxyflavone, a small molecule TrkB agonist, improves spatial memory and increases thin spine density in a mouse model of Alzheimer disease-like neuronal loss. *PLoS One* **9**, e91453, doi:10.1371/journal.pone.0091453 (2014).

20 Cikla, U. *et al.* ERalpha Signaling Is Required for TrkB-Mediated Hippocampal Neuroprotection in Female Neonatal Mice after Hypoxic Ischemic Encephalopathy(1,2,3). *eNeuro* **3**, doi:10.1523/ENEURO.0025-15.2015 (2016).

21 Chen, C. *et al.* The prodrug of 7,8-dihydroxyflavone development and therapeutic efficacy for treating Alzheimer's disease. *Proc Natl Acad Sci U S A* **115**, 578-583, doi:10.1073/pnas.1718683115 (2018).

22 Chen, C. *et al.* Gut dysbiosis contributes to amyloid pathology, associated with C/EBPbeta/AEP signaling activation in Alzheimer's disease mouse model. *Sci Adv* **6**, eaba0466, doi:10.1126/sciadv.aba0466 (2020).

23 Ren, E. *et al.* Functional and Structural Impairments in the Perirhinal Cortex of a Mouse Model of CDKL5 Deficiency Disorder Are Rescued by a TrkB Agonist. *Front Cell Neurosci* **13**, 169, doi:10.3389/fncel.2019.00169 (2019).

24 Wang, Z. H. *et al.* BDNF inhibits neurodegenerative disease-associated asparaginyl endopeptidase activity via phosphorylation by AKT. *JCI Insight* **3**, doi:10.1172/jci.insight.99007 (2018).

25 Wang, Z. H. *et al.* C/EBPbeta regulates delta-secretase expression and mediates pathogenesis in mouse models of Alzheimer's disease. *Nat Commun* **9**, 1784, doi:10.1038/s41467-018-04120-z (2018).

26 Wang, Z. H. *et al.* Deficiency in BDNF/TrkB Neurotrophic Activity Stimulates delta-Secretase by Upregulating C/EBPbeta in Alzheimer's Disease. *Cell Rep* **28**, 655-669 e655, doi:10.1016/j.celrep.2019.06.054 (2019).

27 Compston, J. E., McClung, M. R. & Leslie, W. D. Osteoporosis. *Lancet* **393**, 364-376, doi:10.1016/S0140-6736(18)32112-3 (2019).

28 Windisch, J. M., Marksteiner, R., Lang, M. E., Auer, B. & Schneider, R. Brain-derived neurotrophic factor, neurotrophin-3, and neurotrophin-4 bind to a single leucine-rich motif of TrkB. *Biochemistry* **34**, 11256-11263, doi:10.1021/bi00035a035 (1995).

29 Liu, X. *et al.* Biochemical and biophysical investigation of the brain-derived neurotrophic factor mimetic 7,8-dihydroxyflavone in the binding and activation of the TrkB receptor. *J Biol Chem* **289**, 27571-27584, doi:10.1074/jbc.M114.562561 (2014).

30 Chan, C. B. *et al.* Activation of muscular TrkB by its small molecular agonist 7,8-dihydroxyflavone sex-dependently regulates energy metabolism in diet-induced obese mice. *Chem Biol* **22**, 355-368, doi:10.1016/j.chembiol.2015.02.003 (2015).

31 Fu, Q., Jilka, R. L., Manolagas, S. C. & O'Brien, C. A. Parathyroid hormone stimulates receptor activator of NFkappa B ligand and inhibits osteoprotegerin expression via protein kinase A activation of cAMP-response element-binding protein. *J Biol Chem* **277**, 48868-48875, doi:10.1074/jbc.M208494200 (2002).

32 Kondo, T., Kitazawa, R., Yamaguchi, A. & Kitazawa, S. Dexamethasone promotes osteoclastogenesis by inhibiting osteoprotegerin through multiple levels. *J Cell Biochem* **103**, 335-345, doi:10.1002/jcb.21414 (2008).

33 Song, C. *et al.* Evaluation of efficacy on RANKL induced osteoclast from RAW264.7 cells. *J Cell Physiol* **234**, 11969-11975, doi:10.1002/jcp.27852 (2019).

34 Camerino, C. *et al.* Central depletion of brain-derived neurotrophic factor in mice results in high bone mass and metabolic phenotype. *Endocrinology* **153**, 5394-5405, doi:10.1210/en.2012-1378 (2012).

35 Charatcharoenwitthaya, N., Khosla, S., Atkinson, E. J., McCready, L. K. & Riggs, B. L. Effect of blockade of TNF-alpha and interleukin-1 action on bone resorption in early postmenopausal women. *J Bone Miner Res* **22**, 724-729, doi:10.1359/jbmr.070207 (2007).

36 Poli, V. The role of C/EBP isoforms in the control of inflammatory and native immunity functions. *J Biol Chem* **273**, 29279-29282, doi:10.1074/jbc.273.45.29279 (1998).

37 Ahn, E. H. *et al.* BDNF and Netrin-1 repression by C/EBPbeta in the gut triggers Parkinson's disease pathologies, associated with constipation and motor dysfunctions. *Prog Neurobiol* **198**, 101905, doi:10.1016/j.pneurobio.2020.101905 (2021).

38 Kang, S. S. *et al.* TrkB neurotrophic activities are blocked by alpha-synuclein, triggering dopaminergic cell death in Parkinson's disease. *Proc Natl Acad Sci U S A* **114**, 10773-10778, doi:10.1073/pnas.1713969114 (2017).

39 Xiang, J. *et al.* Delta-secretase-cleaved Tau antagonizes TrkB neurotrophic signalings, mediating Alzheimer's disease pathologies. *Proc Natl Acad Sci U S A* **116**, 9094-9102, doi:10.1073/pnas.1901348116 (2019).

40 Suda, T. *et al.* Regulatory roles of beta-catenin and AP-1 on osteoprotegerin production in interleukin-1alpha-stimulated periodontal ligament cells. *Oral Microbiol Immunol* **24**, 384-389, doi:10.1111/j.1399-302X.2009.00529.x (2009).

41 Zhao, Z. *et al.* Crosstalk between the muscular estrogen receptor alpha and BDNF/TrkB signaling alleviates metabolic syndrome via 7,8-dihydroxyflavone in female mice. *Mol Metab* **45**, 101149, doi:10.1016/j.molmet.2020.101149 (2021).

42 Sun, L. *et al.* FSH directly regulates bone mass. *Cell* **125**, 247-260, doi:10.1016/j.cell.2006.01.051 (2006).

43 Zhu, L. L. *et al.* Blocking antibody to the beta-subunit of FSH prevents bone loss by inhibiting bone resorption and stimulating bone synthesis. *Proc Natl Acad Sci U S A* **109**, 14574-14579, doi:10.1073/pnas.1212806109 (2012).

44 Shirahama-Noda, K. *et al.* Biosynthetic processing of cathepsins and lysosomal degradation are abolished in asparaginyl endopeptidase-deficient mice. *J Biol Chem* **278**, 33194-33199, doi:10.1074/jbc.M302742200 (2003).

45 Li, J. Y. *et al.* Sex steroid deficiency-associated bone loss is microbiota dependent and prevented by probiotics. *J Clin Invest* **126**, 2049-2063, doi:10.1172/JCI86062 (2016).

46 Li, J. Y. *et al.* IL-17A Is Increased in Humans with Primary Hyperparathyroidism and Mediates PTH-Induced Bone Loss in Mice. *Cell metabolism* **22**, 799-810, doi:10.1016/j.cmet.2015.09.012 (2015).

47 Dempster, D. W. *et al.* Standardized nomenclature, symbols, and units for bone histomorphometry: a 2012 update of the report of the ASBMR Histomorphometry Nomenclature Committee. *J Bone Miner Res* **28**, 2-17, doi:10.1002/jbmr.1805 (2013).

Figure legend

Figure 1. AEP knockout improves trabecular bone density in ovariectomy female mice. Femoral bone structures were assessed by *in vitro* μCT in AEP wild-type, AEP Knockout (AEP KO) mice with or without ovariectomy for 8 weeks. (A) Images of the femoral indices of trabecular bone structure measured by *in vitro* μCT scan. (B) μCT scanning measurements of trabecular bone volume fraction (BV/TV), Conn.D., Structure model index (SMI), Trabecular number (Tb.N), Trabecular spacing (Tb.Sp), trabecular thickness (Tb.Th). (n = 5 to 7 mice per group, mean ± SEM, one-way ANOVA, $^{*}P<0.05$, $^{**}P<0.01$). (C) OVX-induced RANKL/OPG ratio is reduced in AEP KO mice. Serum levels of osteocalcin (a marker of bone formation), CTX (a marker of bone resorption), RANK-L, OPG, RANK-L/OPG ratio and serum BDNF level. (n = 5 to 7 mice per group, mean ± SEM, one-way ANOVA, $^{*}P<0.05$, $^{**}P<0.01$)

Figure 2. AEP knockout inhibits the bone turnover induced by ovariectomy in female mice.

(A) Hematoxylin and eosin (H&E) staining of the distal femur bone in AEP WT sham, AEP KO sham, AEP WT OVX and AEP KO OVX group. (Scale bar, 500 μm). (B) Tartrate resistant acid phosphatase-stained (TRAP-stained) sections of the distal femur bone in AEP WT sham, AEP KO sham, AEP WT OVX and AEP KO OVX group were shown at low magnification (upper panel) and higher magnification (lower panel). (Scale bar, 500 μm (upper panel), 20 μm (lower panel)). (C) Mice were injected subcutaneously with calcein at

day 10 and day 3 before sacrifice. Trabecular calcein double-fluorescence labeling images of the representative sections in AEP WT sham, AEP KO sham, AEP WT OVX and AEP KO OVX group (Original magnification × 20). (D) Histomorphometric indices of bone turnover in AEP WT and AEP Knockout mice with or without ovariectomy. MAR and BFR/BS are indices of bone formation, N.Oc/BS and Oc.S/BS are indices of bone resorption. N.Ob/BS, Ob.S/BS are indices of bone formation. MAR = mineral apposition rate; BFR/BS = Bone formation rate; Ob.s/BS = percentage of bone surface covered by osteoblasts; N.Ob/BS = number of osteoblasts per mm bone surface; Oc.S/BS = percentage of bone surface covered by osteoclasts; N.Oc/BS = number of osteoclasts per mm bone surface. (n = 6 mice per group, mean ± SEM, one-way ANOVA, $^{*}P<0.05$, $^{**}P<0.01$)

Figure 3. R13 treatment increases serum OPG levels and blocks trabecular bone loss induced by ovariectomy in both WT and BDNF+/- female mice.

Femoral bone structures were assessed by *in vitro* μCT in wild-type, TrkB+/- and BDNF+/- mice (12 weeks old) with or without ovariectomy, and some of which administrated by R13 (21.8 mg/kg) treatment for 8 weeks (6 days per week) by oral gavage. (A) Images of the femoral indices of trabecular bone structure measured by *in vitro* μCT scan. (B) μCT scanning measurements of trabecular bone volume fraction (BV/TV), Conn.D., Structure model index (SMI), Trabecular number (Tb.N), Trabecular spacing (Tb.Sp), trabecular thickness (Tb.Th). (n = 8 to 9 mice per group, mean ± SEM, one-way ANOVA, $^{*}P<0.05$, $^{**}P<0.01$). (C) R13 decreases RANKL/OPG ratio induced by OVX. Serum levels of osteocalcin, CTX, RANK-L, OPG, RANK-L/OPG ratio and serum BDNF levels. (n = 5 to 7

mice per group, mean ± SEM, one-way ANOVA, $^{*}P<0.05$, $^{**}P<0.01$)

Figure 4. R13 treatment blocks the changes in bone turnover induced by ovariectomy in female mice.

(A) Hematoxylin and eosin (H&E) staining of the distal femur bone in WT sham, BDNF +/- sham, WT OVX, BDNF +/- OVX, and WT OVX + R13, BDNF +/- OVX + R13 group. (Scale bar, 500 μm). (B) Tartrate resistant acid phosphatase-stained (TRAP-stained) sections of the distal femur bone in WT sham, BDNF +/- sham, WT OVX, BDNF +/- OVX, and WT OVX + R13, BDNF +/- OVX + R13 group were shown at low magnification (upper panel) and higher magnification (lower panel). (Scale bar, 500 μm (upper two panels), 20 μm (lower two panels)). (C) Mice were injected subcutaneously with calcein at day 10 and day 3 before sacrifice. Trabecular calcein double-fluorescence labeling images of the representative sections in WT sham, BDNF +/- sham, WT OVX, BDNF +/- OVX, and WT OVX + R13, BDNF +/- OVX + R13 group (Original magnification × 20). (D) Histomorphometric indices of bone turnover in WT and BDNF +/- mice after OVX with or without R13 treatment. N.Oc/BS and Oc.S/BS are indices of bone resorption. N.Ob/BS, Ob.S/BS, MAR and BFR/BS are indices of bone formation. (n = 6 mice per group, mean ± SEM, one-way ANOVA, $^{*}P<0.05$, $^{**}P<0.01$). (E) The schematic diagram of the effect of R13 on osteoporosis.

Figure 5. 7,8-DHF promotes MC3T3-E4 cells differentiation, mineralization and OPG secretion.

(A) ALP staining in MC3T3-E4 cells treated with BDNF or 7,8-DHF for 14 days. (B)

Alizarin Red S mediated calcium staining in MC3T3-E4 cells treated with BDNF or 7,8-DHF for 21 days showed that 7,8-DHF promoted MC3T3 cells mineralization. (C) MC3T3 cells were cultured in complete medium or osteogenic induction medium (OIM) with BDNF or 7,8 DHF for 4 days. Western blotting results showed 7,8-DHF inhibited C/EBPβ/AEP pathway and increase OPG expression. (D) Relative protein level of C/EBPβ, p-C/EBPβ, AEP, RANKL and OPG in MC3T3 cells cultured in complete medium or OIM with BDNF or 7,8 DHF for 4 days; (E) AEP enzymatic activity assay. BDNF and 7,8-DHF inhibited AEP activity. Data represent mean ± SEM of 3 independent experiments ($^{*}P<0.05$, $^{**}P<0.01$, one-way ANOVA). (F) qPCR results showed that OPG mRNA expression increased in MC3T3 cells after 7,8-DHF treatment for 4 days. Data represent mean ± SEM of 3 independent experiments ($^{*}P<0.05$, $^{**}P<0.01$, one-way ANOVA). (G) 7,8-DHF increases OPG and decreases RANKL/OPG ratio. Levels of OPG and RANK-L protein secreted into the medium were measured by ELISA. Data represent mean ± SEM of 3 independent experiments ($^{*}P<0.05$, $^{**}P<0.01$, one-way ANOVA).

Figure 6. 7,8-DHF positively regulates OPG expression via activating CREB.

(A) MC3T3 cells cultured in OIM were treated with 7,8-DHF in different time points. Western blotting showed that 7,8-DHF inhibited C/EBPβ, increased AKT (S473), MAPK (p38), C-Jun, CREB phosphorylation. (B) Relative protein level of C/EBPβ, p- C/EBPβ, AEP, phosphorylated C-Jun, CREB, AKT, MAPK and TrkB in MC3T3 cells treated with 7,8-DHF in different time points. Data represent mean ± SEM of 3 independent experiments ($^{*}P<0.05$, $^{**}P<0.01$, one-way ANOVA). (C) Western blotting showed that knockdown of

CREB blunted 7,8-DHF-induced OPG expression. (D) Relative protein level of RANKL, OPG and RANKL/OPG ratio. Data represent mean ± SEM of 3 independent experiments ($^{*}P<0.05$, $^{**}P<0.01$, one-way ANOVA). (E) qPCR results showed that knockdown of CREB inhibited OPG mRNA expression induced by 7,8-DHF. Data represent mean ± SEM of 3 independent experiments ($^{*}P<0.05$, $^{**}P<0.01$, one-way ANOVA).

Supplementary Figure 1. Ovariectomy induced uterus atrophy in wild type mice. (A) The uterus morphology of the wild-type mice with or without ovariectomy. (B) Uterus weight of the wild-type mice with or without ovariectomy.

Supplementary Figure 2. R13 increases trabecular bone density in wild-type mice. WT mice were treated with or without R13 (21.8 mg/kg) for 8 weeks (6 days per week) by oral gavage at 3 months old. Femoral bone structures were assessed by *in vitro* μCT. (A) Images of the femoral indices of trabecular bone structure measured by *in vitro* μCT scan. (B) R13 increases bone volume fraction in WT mice. μCT scanning measurements of trabecular bone volume fraction (BV/TV), Conn.D., Structure model index (SMI), Trabecular number (Tb.N), Trabecular spacing (Tb.Sp), trabecular thickness (Tb.Th). (n = 8 mice per group, mean ± SEM, one-way ANOVA, $^{*}P<0.05$, $^{**}P<0.01$). (C) R13 elevates OPG levels in WT mice. Serum levels of Osteocalcin, CTX, RANK-L, OPG, RANK-L/OPG ratio and serum BDNF levels. (n = 5 to 7 mice per group, mean ± SEM, one-way ANOVA, $^{*}P<0.05$, $^{**}P<0.01$).

Supplementary figure 3. Blocking AEP activity promotes MC3T3-E4 cell differentiation and mineralization.

MC3T3 cells were cultured in OIM and transfected with or without AEP ^{C189S} plasmid. (A) Western blot showed that AEP ^{C189S} transfection increased fibronectin, osterix, RUNX2 and phosphorylated-CREB expression. (B) AEP ^{C189S} transfection increased ALP staining positive cells in MC3T3 cells cultured in OIM for 14 days. (C) Alizarin Red S mediated calcium staining in MC3T3-E4 cells treated with or without AEP ^{C189S} transfection for 21 days. (D) Relative protein level of AEP, fibronectin, osterix, runx2 and p-CREB/CREB. Data represent mean ± SEM of 3 independent experiments ($^{*}P<0.05$, $^{**}P<0.01$, one-way ANOVA). (E) AEP^{C189S} transfection inhibited AEP activity in MC3T3-E4 cells cultured in OIM.

Supplementary Figure 4. 7,8-DHF inhibits RANK-L-induced RAW264.7 osteoclastogenesis.

(A) TRAP staining of RAW 264.7 cells induced by RANKL with or without BDNF or 7,8-DHF for 4 days. (B& C) Western blotting showed that BDNF and 7,8-DHF inhibited C/EBPβ/AEP pathway, and activated p-TrkB and p-MAPK and p-AKT signaling.

Figures

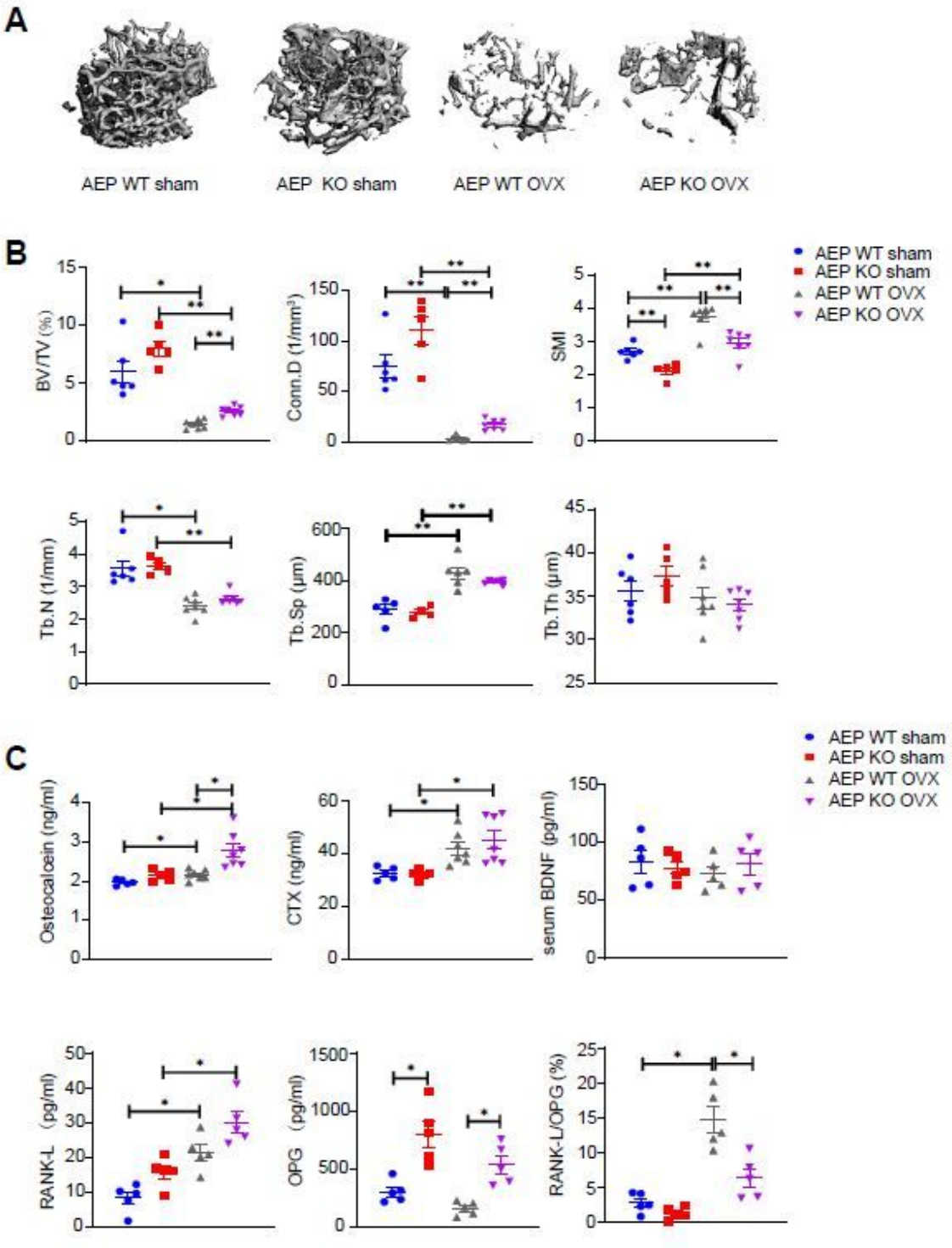

Figure 1

AEP knockout improves trabecular bone density in ovariectomy female mice. Femoral bone structures were assessed by in vitro μCT in AEP wild-type, AEP Knockout (AEP KO) mice with or without ovariectomy for 8 weeks. (A) Images of the femoral indices of trabecular bone structure measured by in vitro μCT

scan. (B) μCT scanning measurements of trabecular bone volume fraction (BV/TV), Conn.D., Structure model index (SMI), Trabecular number (Tb.N), Trabecular spacing (Tb.Sp), trabecular thickness (Tb.Th). (n = 5 to 7 mice per group, mean ± SEM, one-way ANOVA, *P<0.05, ** P<0.01). (C) OVX-induced RANKL/OPG ratio is reduced in AEP KO mice. Serum levels of osteocalcin (a marker of bone formation), CTX (a marker of bone resorption), RANK-L, OPG, RANK-L/OPG ratio and serum BDNF level. (n = 5 to 7 mice per group, mean ± SEM, one-way ANOVA, *P<0.05, ** P<0.01)

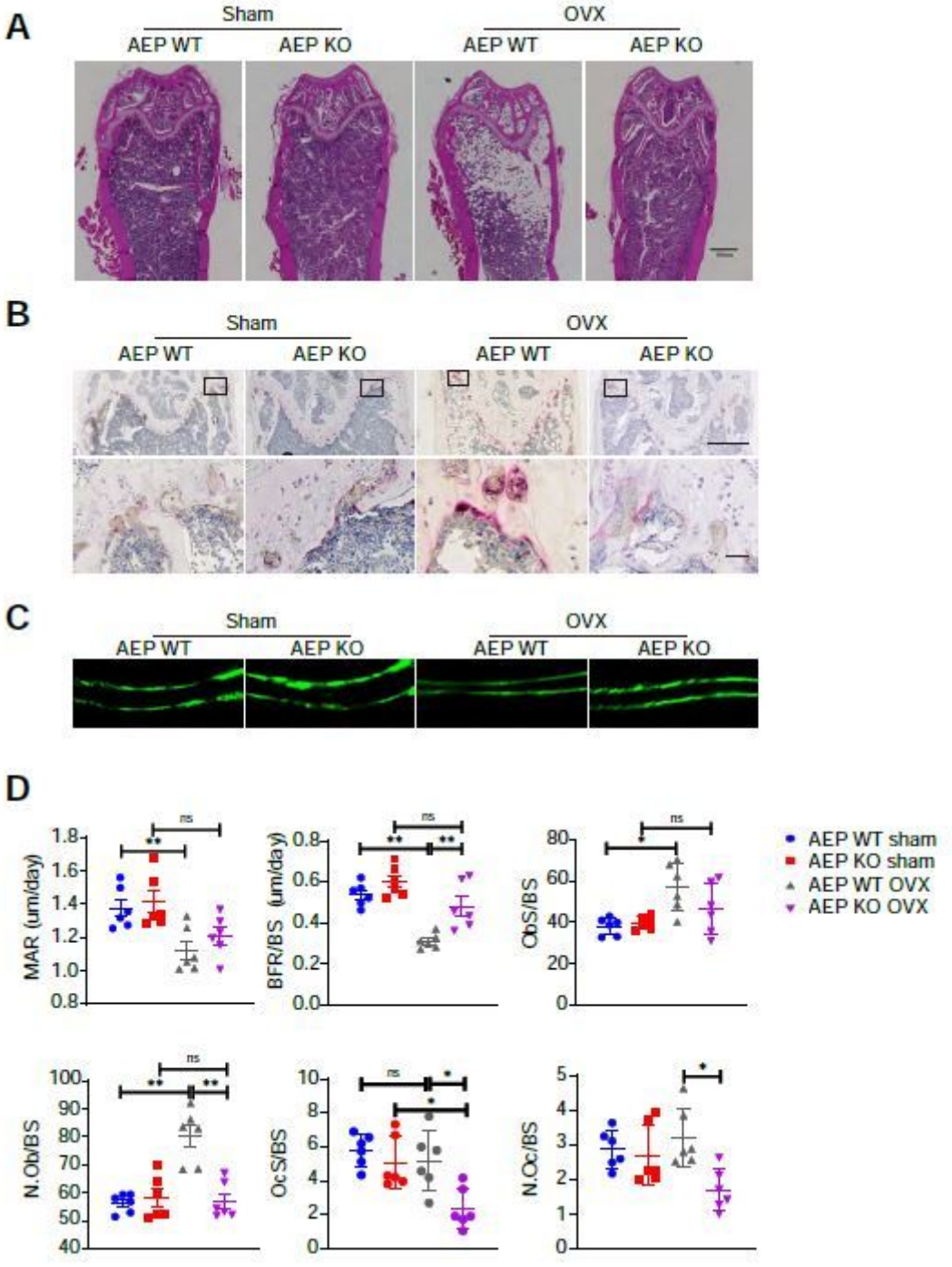

Figure 2

AEP knockout inhibits the bone turnover induced by ovariectomy in female 582 mice. (A) Hematoxylin and eosin (H&E) staining of the distal femur bone in AEP WT sham, AEP KO sham, AEP WT OVX and AEP KO OVX group. (Scale bar, 500 μm). (B) Tartrate resistant acid phosphatase-stained (TRAP-stained) sections of the distal femur bone in AEP WT sham, AEP KO sham, AEP WT OVX and AEP KO OVX group were shown at low magnification (upper panel) and higher magnification (lower panel). (Scale bar, 500 μm (upper panel), 20 μm (lower panel)). (C) Mice were injected subcutaneously with calcein at 25 day 10 and day 3 before sacrifice. Trabecular calcein double-fluorescence labeling images of the representative sections in AEP WT sham, AEP KO sham, AEP WT OVX and AEP KO OVX group (Original magnification × 20). (D) Histomorphometric indices of bone turnover in AEP WT and AEP Knockout mice with or without ovariectomy. MAR and BFR/BS are indices of bone formation, N.Oc/BS and Oc.S/BS are indices of bone resorption. N.Ob/BS, Ob.S/BS are indices of bone formation. MAR = mineral apposition rate; BFR/BS = Bone formation rate; Ob.s/BS = percentage of bone surface covered by osteoblasts; N.Ob/BS = 596 number of osteoblasts per mm bone surface; Oc.S/BS = percentage of bone surface covered by osteoclasts; N.Oc/BS = number of osteoclasts per mm bone surface. (n = 6 mice per group, mean ± SEM, one-way ANOVA, *P<0.05, ** P<0.01)

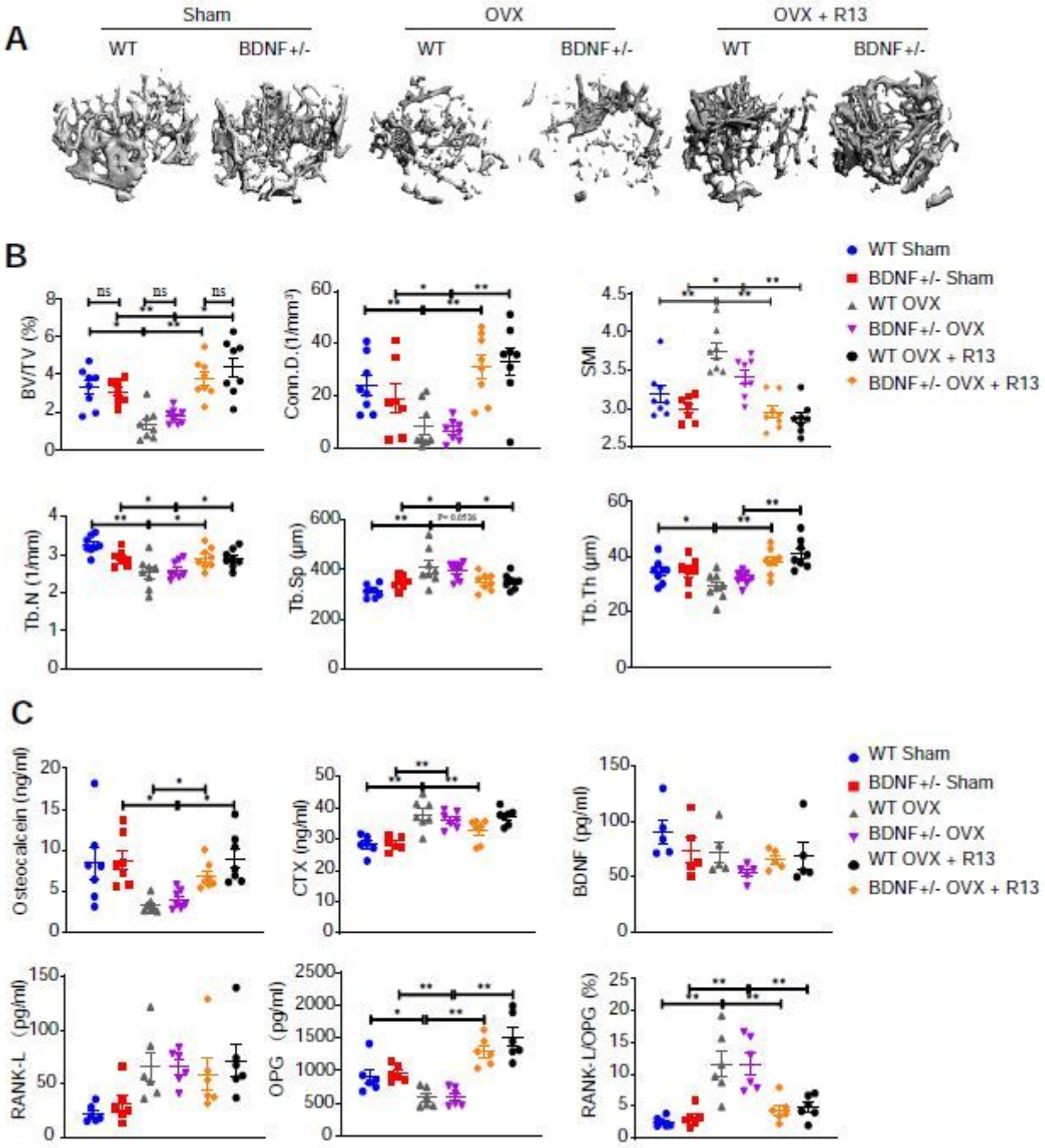

Figure 3

R13 treatment increases serum OPG levels and blocks trabecular bone loss induced by ovariectomy in both WT and BDNF+/- female mice. Femoral bone structures were assessed by in vitro μCT in wild-type, TrkB+/- and BDNF+/- mice (12 weeks old) with or without ovariectomy, and some of which administrated by R13 (21.8 mg/kg) treatment for 8 weeks (6 days per week) by oral gavage. (A) Images of the femoral indices of trabecular bone structure measured by in vitro μCT scan. (B) μCT scanning measurements of trabecular bone volume fraction (BV/TV), Conn.D., Structure model index (SMI), Trabecular number (Tb.N), Trabecular spacing (Tb.Sp), trabecular thickness (Tb.Th). (n = 8 to 9 mice per group, mean ± SEM,

one-way ANOVA, *P<0.05, ** P<0.01). (C) R13 decreases RANKL/OPG ratio induced by OVX. Serum levels of osteocalcin, CTX, RANK-L, OPG, RANK-L/OPG ratio and serum BDNF levels. (n = 5 to 7 26 mice per group, mean ± SEM, one-way ANOVA, *P<0.05, ** P<0.01)

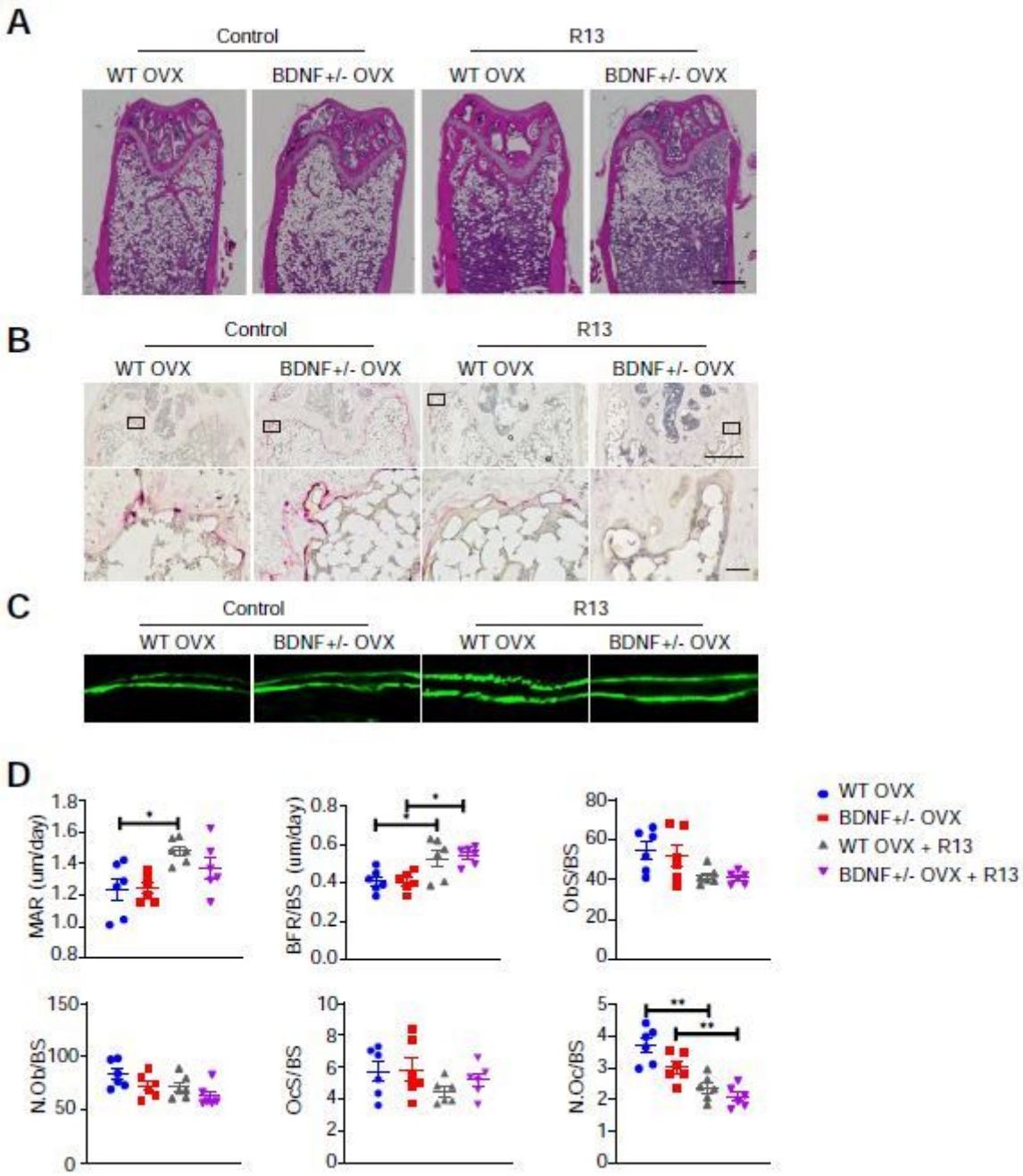

Figure 4

R13 treatment blocks the changes in bone turnover induced by ovariectomy in female mice. (A) Hematoxylin and eosin (H&E) staining of the distal femur bone in WT sham, BDNF +/- sham, WT OVX, BDNF +/- OVX, and WT OVX + R13, BDNF +/- OVX + R13 group. (Scale bar, 500 μm). (B) Tartrate resistant acid phosphatase-stained (TRAP-stained) sections of the distal femur bone in WT sham, BDNF +/- sham,

WT OVX, BDNF +/- OVX, and WT OVX + R13, BDNF +/- OVX + R13 group were shown at low magnification (upper panel) and higher magnification (lower panel). (Scale bar, 500 μm (upper two panels), 20 μm (lower two panels)). (C) Mice were injected subcutaneously with calcein at day 10 and day 3 before sacrifice. Trabecular calcein double-fluorescence labeling images of the representative sections in WT sham, BDNF +/- sham, WT OVX, BDNF +/- OVX, and WT OVX + R13, BDNF +/- OVX + R13 group (Original magnification × 20). (D) Histomorphometric indices of bone turnover in WT and BDNF +/- mice after OVX with or without R13 treatment. N.Oc/BS and Oc.S/BS are indices of bone resorption. N.Ob/BS, Ob.S/BS, MAR and BFR/BS are indices of bone formation. (n = 6 mice per group, mean ± SEM, one-way ANOVA, *P<0.05, ** P<0.01). (E) The schematic diagram of the effect of R13 on osteoporosis.

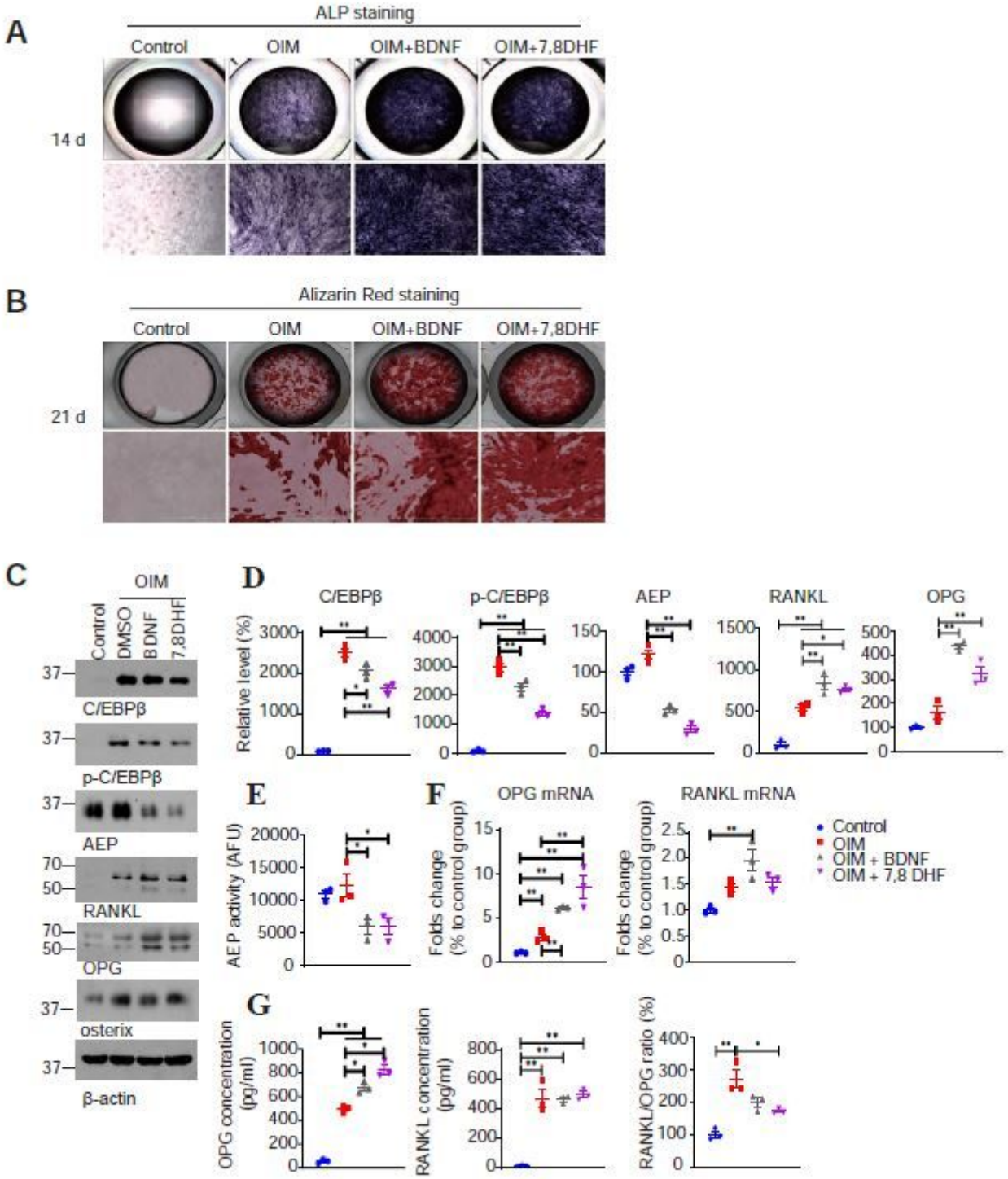

Figure 5

7,8-DHF promotes MC3T3-E4 cells differentiation, mineralization and OPG secretion. (A) ALP staining in MC3T3-E4 cells treated with BDNF or 7,8-DHF for 14 days. (B) 27 Alizarin Red S mediated calcium staining in MC3T3-E4 cells treated with BDNF or 7,8-DHF for 21 days showed that 7,8-DHF promoted MC3T3 cells mineralization. (C) MC3T3 cells were cultured in complete medium or osteogenic induction medium (OIM) with BDNF or 7,8 DHF for 4 days. Western blotting results showed 7,8-DHF inhibited

C/EBPβ/AEP pathway and increase OPG expression. (D) Relative protein level of C/EBPβ, p-C/EBPβ, AEP, RANKL and OPG in MC3T3 cells cultured in complete medium or OIM with BDNF or 7,8 DHF for 4 days; (E) AEP enzymatic activity assay. BDNF and 7,8-DHF inhibited AEP activity. Data represent mean ± SEM of 3 independent experiments (*P<0.05, ** P<0.01, one-way ANOVA). (F) qPCR results showed that OPG mRNA expression increased in MC3T3 cells after 7,8-DHF treatment for 4 days. Data represent mean ± SEM of 3 independent experiments (*P<0.05, ** P<0.01, one-way ANOVA). (G) 7,8-DHF increases OPG and decreases RANKL/OPG ratio. Levels of OPG and RANK-L protein secreted into the medium 645 were measured by ELISA. Data represent mean ± SEM of 3 independent experiments (*P<0.05, ** P<0.01, one-way ANOVA).

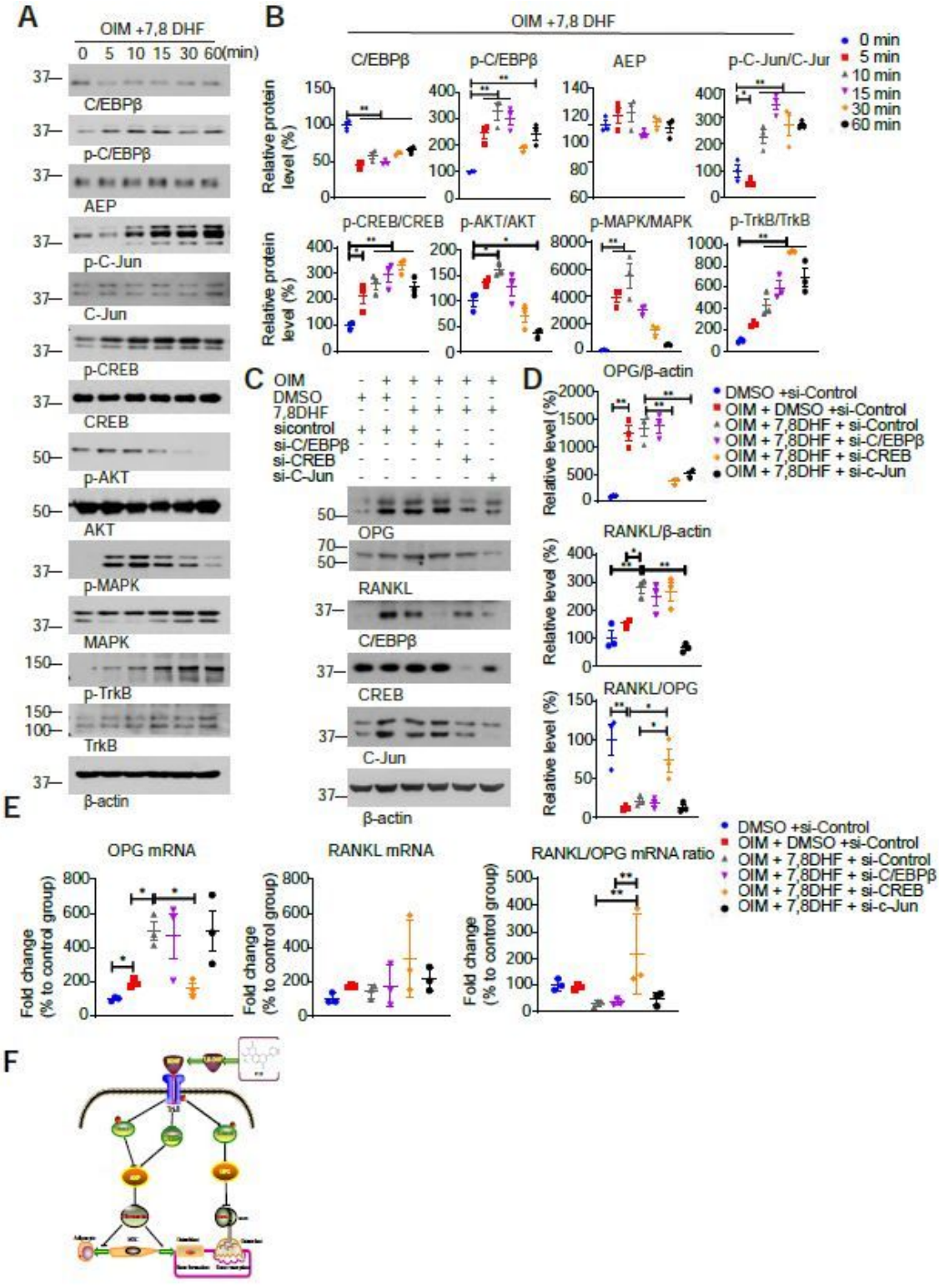

Figure 6

7,8-DHF positively regulates OPG expression via activating CREB. (A) MC3T3 cells cultured in OIM were treated with 7,8-DHF in different time points. Western blotting showed that 7,8-DHF inhibited C/EBPβ, increased AKT (S473), MAPK (p38), C-Jun, CREB phosphorylation. (B) Relative protein level of C/EBPβ, p-C/EBPβ, AEP, phosphorylated C-Jun, CREB, AKT, MAPK and TrkB in MC3T3 cells treated with 7,8- DHF in different time points. Data represent mean ± SEM of 3 independent experiments (*P<0.05, ** P<0.01, one-

way ANOVA). (C) Western blotting showed that knockdown of 28 CREB blunted 7,8-DHF-induced OPG expression. (D) Relative protein level of RANKL, OPG and RANKL/OPG ratio. Data represent mean ± SEM of 3 independent experiments (*P<0.05, ** P<0.01, one-way ANOVA). (E) qPCR results showed that knockdown of CREB inhibited OPG mRNA expression induced by 7,8-DHF. Data represent mean ± SEM of 3 independent experiments (*P<0.05, ** P<0.01, one-way ANOVA).